UNIVERSITY OF TURKU

MASS AND RADIUS CONSTRAINTS FOR NEUTRON STARS USING X-RAY TIMING, SPECTRAL, AND POLARIZATION OBSERVATIONS

Tuomo Salmi

TURUN YLIOPISTON JULKAISUJA – ANNALES UNIVERSITATIS TURKUENSIS
SARJA – SER. AI OSA – TOM. 637 | ASTRONOMICA – CHEMICA – PHYSICA – MATHEMATICA | TURKU 2020

UNIVERSITY OF TURKU

MASS AND RADIUS CONSTRAINTS FOR NEUTRON STARS USING X-RAY TIMING, SPECTRAL, AND POLARIZATION OBSERVATIONS

Tuomo Salmi

TURUN YLIOPISTON JULKAISUJA – ANNALES UNIVERSITATIS TURKUENSIS
SARJA – SER. AI OSA – TOM. 637 | ASTRONOMICA – CHEMICA – PHYSICA – MATHEMATICA | TURKU 2020

University of Turku

Faculty of Science and Engineering
Department of Physics and Astronomy
Astronomy
Doctoral Programme in Physical and Chemical Sciences

Supervised by

Prof. Juri Poutanen
Department of Physics and Astronomy
University of Turku
Turku, Finland

Docent Sergey Tsygankov
Department of Physics and Astronomy
University of Turku
Turku, Finland

PhD Joonas Nättilä
Physics Dept. and Astrophysics Lab.
Columbia University & Flatiron Institute
New York, USA

Reviewed by

Prof. Denis Leahy
Department of Physics and Astronomy
University of Calgary
Calgary, Canada

Prof. Stephan Rosswog
Astronomy and Oskar Klein Centre
Stockholm University
Stockholm, Sweden

Opponent

Prof. Marat Gilfanov
Max Planck Institute for Astrophysics
Garching, Germany

& Space Research Institute
& Moscow, Russia

The originality of this publication has been checked in accordance with the University of Turku quality assurance system using the Turnitin OriginalityCheck service.

ISBN 978-951-29-8277-6 (PRINT)
ISBN 978-951-29-8278-3 (PDF)
ISSN 0082-7002 (Print)
ISSN 2343-3175 (Online)
Painosalama Oy - Turku, Finland 2020

Acknowledgements

First, I would like to thank my supervisors Prof. Juri Poutanen, Drs. Joonas Nättilä and Sergey Tsygankov. Their guidance was crucial in conducting the research, writing the thesis, and getting practised in the academic life. The journey, started as a master's project, turned out to be a pleasant and still continuing experience.

I would also like to thank Profs. Stephan Rosswog and Denis Leahy for their profound pre-examination of this thesis. In addition, I gratefully acknowledge Prof. Marat Gilfanov for agreeing to become my opponent at the thesis defence. I also thank the University of Turku Graduate School and Magnus Ehrnrooth foundation for their financial support of my PhD thesis work.

Besides my supervisors, many collaborators have strongly influenced the work done in this thesis. First of all, I thank Valery Suleimanov, who contributed substantially to the research and kindly hosted my visits to the University of Tübingen. I am also grateful for Joonas and the other people at Nordita for my useful Visiting PhD Fellowship. Furthermore, I thank all the other collaborators, including Vlad Loktev, Karri Korsman, Luca Baldini, Cole Miller, Andrew Steiner, Anna Watts, and Pauli Pihajoki, to name a few.

I would also like to give my deep appreciation for the high-energy astrophysics group of University of Turku. Besides those already mentioned, I thank Alexandra, Andrei, Anna, Armin, Juhani, Ilia, Pavel, Vadim, and Yasir. I would also like to extend my gratitude for all the other (current and previous) members of Tuorla Observatory, who created an inspiring and supportive working atmosphere. Especially, I thank the Tuorla Board Game Club and Kalle for organizing the exciting game events.

Finally, I would like to thank my family and friends for all their support. Most importantly, I thank my wife Laura and daughter Ella for their love and encouragement.

Contents

Abstract

Neutron stars (NSs) are the most dense objects in the Universe that can be directly observed. The nature of the cold ultra-dense matter inside them is still unresolved, and determining the equation of state (EoS) of that matter is a fundamental problem in nuclear physics. Measurements of sizes and masses of NSs can be used to constrain the EoS, and thus NSs can be described as astrophysical laboratories for nuclear physics.

The size (or radius) and mass measurements can be done, for example, using the X-ray timing observations of millisecond pulsars (MSPs), which are very rapidly rotating NSs. In the first part of this thesis, I have presented a framework that can be used to model the observed X-ray pulse profiles from MSPs and to obtain constraints for the model parameters, including NS mass and radius. I have also estimated how the upcoming X-ray polarization measurements will improve the constraints. In addition, I have shown that there also exist problems in the current models in explaining all the features of the X-ray data. Especially, the emission pattern from an atmosphere of an accretion-powered millisecond pulsar (AMP) should be accurately solved for more robust estimates.

Moreover, modelling NS atmospheres is not only important for AMPs, but also essential for pulse profile modelling of rotation-powered millisecond pulsars (RMPs), and that is considered in the second part of the thesis. I have studied the importance of the exact formulation of Compton scattering in the RMP atmospheres and created a novel model for RMP atmospheres heated by magnetospheric return-currents. This model differs from the preceding ones in that it does not assume that all the heat is released in the deepest layers of the atmosphere. The results imply that the emission pattern also from RMP surface may significantly deviate from that predicted by previous models, which could affect also the recent radius constraints obtained from the observations of Neutron star Interior Composition ExploreR (NICER) instrument.

In the final part of the thesis, I have studied, in more detail, how the

upcoming X-ray polarization observations of rapidly rotating NSs can be accurately modelled accounting for the flattened shape of the star and used to obtain further constraints on the EoS of ultra-dense matter. The results show that the unknown physics of NS interiors can be probed by combining X-ray timing, spectral, and polarization measurements of MSPs.

Tiivistelmä

Neutronitähdet ovat maailmankaikkauden tiheimpiä suoraan havaittavia kohteita. Niiden sisällä olevan erittäin tiheän kylmän aineen olemus on yhä selvittämättä, ja kyseistä ainetta kuvaavan tilanyhtälön ratkaiseminen on perustavanlaatuinen ongelma ydinfysiikassa. Neutronitähtien massoja ja säteitä mittaamalla voidaan rajata tilanyhtälöä, ja täten neutronitähtien voidaankin sanoa olevan ydinfysiikan astrofysikaalisia laboratiorioita.

Neutronitähden kokoa (tai sädettä) ja massaa voidaan mitata hyödyntämällä esimerkiksi röntgen-ajoitus havaintoja millisekuntipulsareista, jotka ovat hyvin nopeasti pyöriviä neutronitähtiä. Väitöskirjan ensimmäisessä osassa olen esittänyt menetelmän, jota voidaan käyttää havaittujen röntgenpulssien mallintamiseen ja tähden parametrien, kuten massan ja säteen, rajaamiseeen. Olen myös arvioinut kuinka tulevat röntgen-polarisaatiomittaukset auttavat massan ja säteen rajaamisessa. Lisäksi olen osoittanut, että nykyisillä malleilla on vaikea selittää kaikkia röntgen-havaintojen yksityiskohtia. Erityisesti neutronitähden ilmakehän säteilymalli aineen kertymisestä voimansa saavissa millisekuntipulsareissa (accretion-powered millisecond pulsars, AMP) pitäisi ratkaista tarkemmin luotettavampia arvioita varten.

Neutronitähtien ilmakehien mallintaminen ei ole tärkeää vain AMP:ille, vaan se on keskeistä myös pyörimisestä voimansa saaville millisekuntipulsareille (rotation-powered millisecond pulsars, RMP), ja sitä käsitelläänkin väitöskirjani toisessa osassa. Olen tutkinut Compton sironnan tarkan esityksen tärkeyttä RMP:iden ilmakehämalleissa ja luonut myös uuden mallin kuvaamaan magnetosfäärisen paluuvirran lämmittämiä RMP:iden ilmakehiä. Tämä malli eroaa aiemmmista siinä, että se ei oleta kaiken lämmön vapautuvan ilmakehän syvimmissä kerroksissa. Tulokset osoittavat, että myös RMP:n säteilymalli voi erota merkittävästi aiemmista ennustuksista, mikä voi vaikuttaa myös tuoreisiin Neutron star Interior Composition ExploreR (NICER) -instrumentin havaintojen perusteella tehtyihin neutronitähden säteen mittauksiin.

Väitöskirjan viimeisessä osassa olen tutkinut aiempaa tarkemmin miten pian tehtäviä röntgen-polarisaatio havaintoja nopeasti pyörivistä neutronitähdistä voidaan mallintaa riittävällä tarkkuudella ottaen huomioon tähden litistynyt muoto ja miten niitä voidaan hyödyntää tiheän aineen tilanyhtälön rajaamisessa. Tulokset osoittavat, että neutronitähtien sisäosien tuntematonta fysiikkaa voidaan luodata yhdistämällä millisekuntipulsareiden röntgen ajoitus-, spektri- ja polarisaatio-havaintoja.

List of publications

I Bayesian parameter constraints for neutron star masses and radii using X-ray timing observations of accretion-powered millisecond pulsars,
T. Salmi, J. Nättilä, and J. Poutanen, A&A **618**, A161 (2018), https://doi.org/10.1051/0004-6361/201833348.

II Effects of Compton scattering on the neutron star radius constraints in rotation-powered millisecond pulsars,
T. Salmi, V. F. Suleimanov, and J. Poutanen, A&A **627**, A39 (2019), https://doi.org/10.1051/0004-6361/201935442.

III Magnetospheric return-current-heated atmospheres of rotation-powered millisecond pulsars,
T. Salmi, V. F. Suleimanov, J. Nättilä, and J. Poutanen, A&A **641**, A15 (2020), https://doi.org/10.1051/0004-6361/202037824.

IV Oblate Schwarzschild approximation for polarized radiation from rapidly rotating neutron stars,
V. Loktev, *T. Salmi*, J. Nättilä, and J. Poutanen, A&A, **643**, A84 (2020), https://doi.org/10.1051/0004-6361/202039134.

V Neutron star parameter constraints for accretion-powered millisecond pulsars from the simulated IXPE data,
T. Salmi, V. Loktev, K. Korsman, L. Baldini, S. S. Tsygankov, and J. Poutanen, A&A, in press (2020), https://arxiv.org/abs/2009.09744.

Additional publications not included in the thesis

Evidence for the Photoionization Absorption Edge in a Photospheric Radius Expansion X-Ray Burst from GRS 1747−312 in Terzan 6,
Z. Li, V. Suleimanov, J. Poutanen, *T. Salmi*, M. Falanga, J. Nättilä, and R. Xu, ApJ **866**, 53 (2018), `https://doi.org/10.3847/1538-4357/aade8e`.

Dense matter with eXTP,
A. L. Watts, W. Yu, J. Poutanen, S. Zhang, S. Bhattacharyya, S. Bogdanov, L. Ji, A. Patruno, T. E. Riley, and et al. (incl. *T. Salmi*), *Science China Physics, Mechanics, and Astronomy* **62**, 29503 (2019), `https://doi.org/10.1007/s11433-017-9188-4`.

Observatory science with eXTP,
J. J. M. in't Zand, E. Bozzo, J. Qu, X.-D. Li, L. Amati, Y. Chen, I. Donnarumma, V. Doroshenko, S. A. Drake, and et al. (incl. *T. Salmi*), *Science China Physics, Mechanics, and Astronomy* **62**, 29506 (2019), `https://doi.org/10.1007/s11433-017-9186-1`.

The X-ray Polarization Probe mission concept,
K. Jahoda, H. Krawczynski, F. Kislat, H. Marshall, T. Okajima, I. Agudo, L. Angelini, M. Bachetti, L. Baldini, and et al. (incl. *T. Salmi*), *Astrophysics Decadal Survey*, submitted (2019), `https://arxiv.org/abs/1907.10190`.

List of abbreviations

AMP	accretion-powered millisecond pulsar
EoS	equation of state
eXTP	enhanced X-ray Timing and Polarimetry mission
IXPE	Imaging X-ray Polarimeter Explorer
MCMC	Markov Chain Monte Carlo
MSP	millisecond pulsar
NICER	Neutron star Interior Composition ExploreR
NS	neutron star
PA	polarization angle
PD	polarization degree
RMP	rotation-powered millisecond pulsar
RXTE	Rossi X-ray Timing Explorer

Chapter 1

Introduction

1.1 Neutron stars

Neutron stars (NSs) are very dense cores of collapsed dying massive stars. They form as remnants of supernova explosions of stars, which have mass between $8\,M_\odot$ and $25\,M_\odot$ (solar masses). In less massive stars, the electron degeneracy pressure supports against the gravitational collapse (electrons can not be packed closer to each other), and a less compact white dwarf is formed without supernova explosion. When the core is massive enough, the collapse can overcome this pressure and positive protons (in the centre of the atoms) will come in contact with surrounding negative electrons and create neutral neutrons. In the most massive stars ($> 25\,M_\odot$), the collapse will overcome even the degeneracy pressure of neutrons and the repulsive nuclear forces, which mainly support the NS against gravity, and the remnant will collapse into a black hole instead.

The precise masses, ranging from $1.17\,M_\odot$ to $2.14\,M_\odot$, have been measured for a few tens of NSs located in binary systems (Martinez et al. 2015; Özel & Freire 2016; Cromartie et al. 2020). Recent gravitational wave observations (named as GW190814) from the coalescence of a black hole and a compact object, possibly a NS, suggest even a NS mass of $2.6\,M_\odot$ (Abbott et al. 2020). Generally, accretion from a companion star is expected to have increased the NS mass from the initial mass of the collapsed core. Since the radius of the NS is typically proposed to be about 12 km, it is evident that NSs are the most dense objects in the Universe that can be directly observed. The supranuclear densities of the matter inside the star can currently be produced in Earth laboratories only in ultrarelativistic heavy-ion collisions at high temperatures (Gyulassy & McLerran 2005; An-

dronic et al. 2018). Astrophysical observations of NSs are thus essential in order to understand the properties of this matter at low temperatures. As expected, neutrons most likely dominate the nucleonic content of NSs. In addition, some protons, electrons, and muons are believed to exist inside NSs (Haensel et al. 2007). However, the composition of the innermost core of the NS is still unknown and exotic baryons, mesons or quarks could also appear (see e.g. Annala et al. 2020). To understand the composition and properties better, we need to determine what is the equation relating the thermodynamic quantities of the dense matter.

1.2 Equation of state

The relation between pressure P, density ρ, and temperature T (generally also together with other state variables like entropy density and particle species number densities) is described by the equation of state (EoS). For the dense matter inside the NS, we usually need only a function connecting pressure and (mass) density $P(\rho_{\mathrm{m}})$, since the pressure is dominated by the repulsive nuclear interactions and the quantum mechanical effects resulting from the effectively cold degenerate matter. However, there is significant amount of uncertainty in the exact form of the EoS due to the poorly constrained many-body interactions in the high-density regime (Lattimer & Prakash 2001).

The densities in the cores of NSs may reach up to ten times the nuclear saturation density $\rho_{\mathrm{sat}} \simeq 2.7 \times 10^{14}\mathrm{g/cm}^3$ (Baym et al. 2018). The microphysical behaviour of dense matter is not well understood in this density regime. As already mentioned, comparable densities can be studied with heavy ion collision experiments, but only at high temperatures. Theoretical calculations at low temperatures, comparable to NS cores, can be attained only at sub-saturation densities (Hebeler et al. 2010). On the other hand, perturbative modelling of quantum chromodynamics (theory of strong interactions) can also give some EoS constraints, but only for higher densities than several times the density of NS core (Kurkela et al. 2014). Thus, NSs are unique laboratories to study the nature of weak and strong interactions in dense matter and simultaneously obtain information of the composition of the NS.

The EoS, which describes the microphysics in the dense matter, can also be examined using the compressibility of the star. With higher compress-

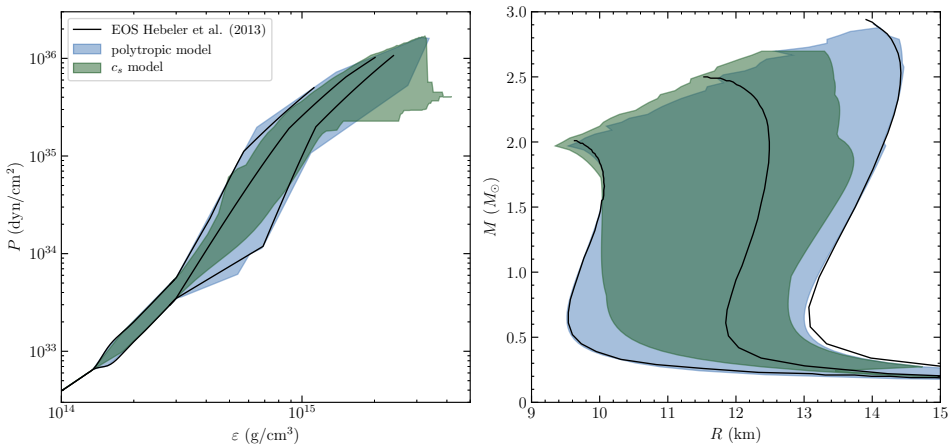

Figure 1.1: Range for the EoS (*left panel*) fulfilling the parameter bounds described in Greif et al. (2019) and the corresponding range for the NS mass-radius relations (*right panel*). The ranges are shown for two different EoS parametrisation: Piecewise polytropic model (PP; Hebeler et al. 2013) shown in light blue and speed of sound (CS) model shown in green. The black lines show three representative EoS of the PP model. Taken from Greif et al. (2019).

ibility (determined using the gradient of EoS), we obtain a smaller radius of the most massive NS that can be supported (Stergioulas 2003). The mapping between EoS and the observed mass and radius can also be described by the equation for hydrostatic equilibrium (Lattimer & Prakash 2004). For a general relativistic and spherically symmetric (non-rotating) object, these equations can be read as (Tolman 1934; Oppenheimer & Volkoff 1939):

$$\frac{\mathrm{d}P}{\mathrm{d}r} = -\frac{G[m(r) + 4\pi r^3 P/c^2](\rho_\mathrm{m} + P/c^2)}{r[r - 2Gm(r)/c^2]}, \tag{1.1}$$

and

$$\frac{\mathrm{d}m(r)}{\mathrm{d}r} = 4\pi\rho_\mathrm{m} r^2, \tag{1.2}$$

where $m(r)$ is the gravitational mass enclosed within a radius r, G is the gravitational constant, and c is the speed of light. Thus, there is a one-to-

one mapping between the pressure-density and mass-radius relations and constraints on the latter can be used to constrain the EoS. The connection between the parameters is also demonstrated in Fig. 1.1, where the pressure P is expressed as a function of energy density ϵ instead of mass density ρ_{m}. In the next section, we will describe the astrophysical sources that are expected to be good candidates to measure the NS mass and radius with the required accuracy.

1.3 Millisecond pulsars

Millisecond pulsars are a class of most rapidly rotating NSs, which are valuable targets when aiming to constrain the mass and radius of the NS (Poutanen & Gierliński 2003; Özel 2013; Watts et al. 2016, 2019). Two different groups of them are considered next.

1.3.1 Accretion-powered millisecond pulsars

Accretion-powered millisecond pulsars (AMPs) are rapidly rotating NSs in binary systems (in so-called low-mass X-ray binaries) where the gas from a relatively low-mass companion star is stripped to an accretion disk and then channelled onto the magnetic poles of the NS. As a result, we can detect X-ray pulses from the pair of the 'hot spots' formed on the surface of the pulsar. Typical observed periods are in the order of few milliseconds and correspond to the spin frequency of the NS.

The high spin frequency of the AMPs can be explained by accretion torques (transfer of angular momentum via accretion from the companion) that are believed to have reduced the pulsar rotation period from seconds to milliseconds (Alpar et al. 1982; Radhakrishnan & Srinivasan 1982). In addition, the original surface magnetic field is typically reduced from 10^{12} G to 10^{8} G. Observations by Rossi X-ray Timing Explorer (RXTE) were used to detect first persistent millisecond pulsations in X-ray flux from an accreting source SAX J1808.4−3658 (Wijnands & van der Klis 1998). This was considered to be the missing evolutionary link between the previously discovered (rotation-powered) millisecond pulsars having no signs of accretion from the companion, and the 'normal' pulsars.

The observed X-ray radiation from AMPs is thought to be produced by thermal emission from the heated hot spots that is reprocessed (by Compton scattering) when going through an accretion column formed above the

spot. This reprocessing Comptonizes the blackbody photons and is responsible for the power-law spectra observed up to 100 keV (Poutanen & Gierliński 2003). However, understanding the exact details of the spectrum and angular distribution of emission requires rigorous modelling of the physics of the interaction between radiation and matter in the accretion column. Usually, only simplifying assumptions about the accretion column have been applied (Poutanen & Gierliński 2003; Leahy et al. 2008; Salmi et al. 2018), including circular spots on the surface of the NS with homogenous temperature structure, approximate formulas for the anisotropy of the radiation, and empirical models for Comptonized spectra (Steiner et al. 2009). A detailed analysis is still left for a future work. Valuable information of the mass and radius (and thus EoS) may still be obtained from the light curves, mainly due to the light bending and thus pulse shape, which strongly depend on the compactness of the star (Poutanen 2008).

1.3.2 Rotation-powered millisecond pulsars

Rotation-powered millisecond pulsars (RMPs), also known as radio millisecond pulsars, are rapidly rotating NSs that, similarly to AMPs, have been spun-up due to the accretion from a companion star, but where the accretion has ceased. They are mostly observed in radio wavelengths due to the non-thermal emission from their magnetosphere. However, later there have also been detections of thermal soft X-ray emission (Grindlay et al. 2002; Zavlin 2006, 2007), pulsating at the spinning frequency of the NS. The observed spectra and pulse shapes differ significantly from AMPs, but the emission is again believed to originate from hot spots on the NS surface. This enables obtaining mass and radius constraints using pulse profile modelling also for these sources.

The difference in the emission pattern of AMPs and RMPs is expected to arise from a different heating mechanism of the hot spots. After transiting from the accretion-powered to rotation-powered phase, the polar caps of the NS are not heated by the accretion of the atoms from the companion, but by the bombardment of relativistic electrons and positrons from a magnetospheric return current instead (see e.g. Zel'dovich & Shakura 1969; Alme & Wilson 1973; Ruderman & Sutherland 1975; Arons 1981; Zampieri et al. 1995; Harding & Muslimov 2001). The magnetospheric current is created by magnetic field together with the rotation of the star. Electrons are first released from the surface of the star and then accelerated to relativistic

speeds. These high velocity particles emit gamma rays that produce pairs of electrons and positrons, out of which some travel back to the NS and heat its atmosphere. The temperature of the RMP atmosphere is generally lower than in AMPs, and due to lack of radiation re-processing in accretion column, modelling the spectrum and angular distribution of radiation is less complicated. However, even in this case, we have developed a new atmosphere model that overcomes the usual, probably inaccurate, assumption of energy released only in the deep layers of the atmosphere (see Chapter 3). This is expected to be important for obtaining reliable mass and radius estimates when applying the spectral and beaming model in pulse profile calculation (see Chapter 2).

Chapter 2

Pulse profile modelling of neutron stars

Let us next discuss how modelling the X-ray pulses of NSs can be used to constrain their masses and radii, and thus the EoS. We concentrate on pulse profiles of the two different types of NSs introduced in the previous chapter: AMPs and RMPs. The techniques to model the photon trajectories from the stellar surface to the observer (in general relativity), can also be applied, for example, in case of millisecond pulsars that are powered by thermonuclear bursts or in case of slower rotation-powered pulsars. However, the time and energy dependence of the radiation are connected to the details of the radiative transfer on and above the heated NS surface and should be considered for each type of system separately.

If we would prefer to compute the pulse profiles with best possible accuracy, we should solve the exact general relativistic equations for the stellar shape and the metric of the space-time by using, for example, a Rapidly Rotating Neutron star (RNS) model presented by Stergioulas & Friedman (1995). Then the photon trajectories should be traced numerically using a relativistic ray-tracing algorithm (see e.g. Nättilä & Pihajoki 2018; Pihajoki et al. 2018; Vincent et al. 2018). However, speed of the calculation is also essential for statistical inference, since a vast number of pulses must be computed in order to obtain NS parameter constraints. Therefore, we have adopted an approximate Schwarzschild description of the space-time, accounting separately for special relativistic Doppler effect and aberration (see e.g. Pechenick et al. 1983; Miller & Lamb 1998; Nath et al. 2002; Poutanen & Gierliński 2003; Poutanen & Beloborodov 2006), and used an analytical model for the oblate shape of the star (AlGendy & Morsink 2014, but see

also Silva et al. 2020 for a revised expression). The model has been shown to be computationally fast but still highly accurate. The main features of this approach, also called 'oblate Schwarzschild' (OS) approximation, are introduced in the following sections (see also Morsink et al. 2007; Miller & Lamb 2015; Bogdanov et al. 2019; Suleimanov et al. 2020).

In addition, there are a number of other methods, based on astrophysical observations, that can be independently used to constrain the NS mass and radius. These include, spectral modelling of the X-ray bursting NSs described, for example, by Nättilä et al. (2017), a variety of other methods based on electromagnetic observations (see Degenaar & Suleimanov 2018, for a review), and measuring the star's tidal deformability from the gravitational wave emission of NS-NS merger events (see e.g. Abbott et al. 2018; Annala et al. 2018; Capano et al. 2020). Combining different techniques allows to obtain more precise constraints for the NS EoS (Raaijmakers et al. 2020; Miller et al. 2020; Al-Mamun et al. 2020).

We begin by discussing the geometrical effects that need to be taken into account when modelling the pulse shapes. We continue by describing the method used to simulate the photon trajectories in a relativistic space-time. The chapter is finished by outlining the connection between the light-ray tracing, physics of NS atmosphere, and the observed flux. We also briefly introduce the procedure of constraining the model parameters from X-ray data using Bayesian analysis.

2.1 Geometry of the star

The first concept to examine is the shape of the NS. In case of millisecond pulsars, the shape is oblate instead of spherical, since the star is flattened from its poles due to the fast rotation. Fortunately, the relation between the shape of the star and the NS gravitating mass M, equatorial radius $R_{\rm eq}$, and spin period P, has been found to be highly universal with only an implicit dependence on the EoS (Morsink et al. 2007; AlGendy & Morsink 2014), in case of moderate spin frequencies of the star ($\nu \lesssim 700$ Hz). The radius of the star as a function of co-latitude $R(\theta)$ (measured from the spin axis) can be obtained from (AlGendy & Morsink 2014)

$$\frac{R(\theta)}{R_{\rm eq}} = 1 + o_2(x, \bar{\Omega}) \cos^2 \theta, \tag{2.1}$$

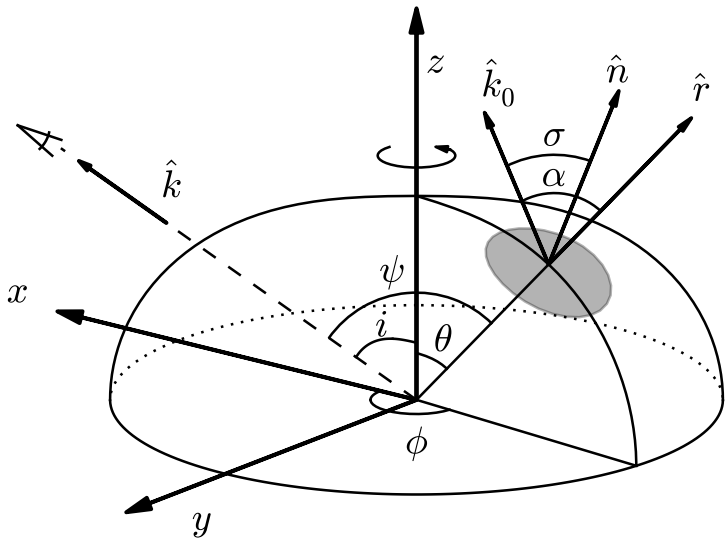

Figure 2.1: Geometry of the star. The Cartesian (x, y, z) and spherical (with θ and ϕ) coordinate systems are shown. Due to the oblate shape, the radial vector $\hat{r}$ and the surface normal $\hat{n}$ are not equal. The photon from the hot spot is initially emitted towards $\hat{k}_0$ but due to the light bending it reaches the observer in direction of $\hat{k}$. Taken from Salmi et al. (2018).

where

$$o_2(x, \bar{\Omega}) = \bar{\Omega}^2(-0.788 + 1.030x), \tag{2.2}$$

$$x = \frac{GM}{c^2 R_{\rm eq}}, \tag{2.3}$$

and

$$\bar{\Omega} = \frac{2\pi}{P}\left(\frac{R_{\rm eq}^3}{GM}\right)^{1/2}. \tag{2.4}$$

The effect of fast rotation on the shape of the NS is important when the spinning frequency is more than about 300 Hz (Cadeau et al. 2007). In that case, the pulse profiles are altered since the visibility of the hot spot to the observer for an oblate star is different from that of a spherical star. An illustration of the geometry of the star is shown in Fig 2.1, where we also define the fundamental angles and vectors of the system. Observer inclination i and co-latitude of the emitting point θ (measured from the rotation pole) are assumed to be time-independent. However, as the star rotates (meaning that the phase angle ϕ of the emitting point changes) the observer sees photons which are emitted at different angles σ relative to the surface normal, or at angles α relative to the radial direction. For each moment we know that the light must bend in angle ψ (relative to the radial direction), determined from

$$\cos\psi = \cos i \ \cos\theta + \sin i \ \sin\theta\cos\phi, \tag{2.5}$$

in order to be detected by the observer. The corresponding emission angle (either σ or α) can be resolved using general relativity (see Sect. 2.2). However, if the emission angle σ is required to be more than $\pi/2$, the photon would have to penetrate through the star and it thus can not be observed. Clearly, this condition does not always simultaneously appear in oblate and spherical stars. In principle, the photon might also be hindered by the surface of the star at a later point of its trajectory if the star is oblate.

The relation between the two emission angles (identical only for spherical stars) is obtained as (Morsink et al. 2007)

$$\cos\sigma = \cos\alpha\cos\gamma + \frac{\sin\alpha}{\sin\psi}\sin\gamma(\cos i\sin\theta - \sin i\cos\theta\cos\phi), \tag{2.6}$$

where γ is the angle between surface normal and radial vectors, and it is obtained from

$$\cos\gamma = \frac{1}{\sqrt{1+f^2(\theta)}} \quad \text{and} \quad \sin\gamma = \frac{f(\theta)}{\sqrt{1+f^2(\theta)}}, \tag{2.7}$$

where the function $f(\theta)$ is given by

$$f(\theta) = \frac{1}{R\sqrt{1-u}}\frac{\mathrm{d}R}{\mathrm{d}\theta}, \tag{2.8}$$

where $u = R_\mathrm{S}/R$, $R_\mathrm{S} = 2GM/c^2$ is the Schwarzschild radius, $R = R(\theta)$ is the circumferential radius of the star at the point where the photon is emitted, and the derivative $\mathrm{d}R/\mathrm{d}\theta$ depends on the spin frequency as seen from Eq. (2.1). However, due to rapid rotation and relativistic aberration, the angles seen by the distant observer differ from those measured in the comoving frame of the spot (see Section 2.2).

2.2 Light bending and relativity

Next we consider the relation between the emission angle α and the light bending angle ψ. If assuming a Schwarzshchild geometry (i.e. neglecting rotational effects on the space-time) the relation between these variables (when $\alpha < \pi/2$) is given by (Misner et al. 1973; Pechenick et al. 1983)

$$\psi_\mathrm{p}(R,\alpha) = \int_R^\infty \frac{\mathrm{d}r}{r^2}\left[\frac{1}{b^2} - \frac{1}{r^2}\left(1 - \frac{R_\mathrm{S}}{r}\right)\right]^{-1/2}, \tag{2.9}$$

where b is the impact parameter:

$$b = \frac{R}{\sqrt{1-u}}\sin\alpha. \tag{2.10}$$

It is thus apparent, that the bending of the photon encodes information of the NS mass and radius. In case of $\alpha > \pi/2$, the photon trajectory will initially have a decreasing radial coordinate (possible for an oblate star as long as $\sigma < \pi/2$), and the relation between α and ψ is (Poutanen 2020a)

$$\psi(R,\alpha) = 2\psi_\mathrm{max} - \psi_\mathrm{p}(R,\pi-\alpha), \tag{2.11}$$

where $\psi_\mathrm{max} = \psi_\mathrm{p}(\mathsf{p},\alpha = \pi/2)$ and p is the periastron (closest distance to the centre of the star of the photon trajectory), given by

$$\mathsf{p} = -\frac{2}{\sqrt{3}}b\cos([\arccos(3\sqrt{3}R_\mathrm{S}/(2b)) + 2\pi]/3). \tag{2.12}$$

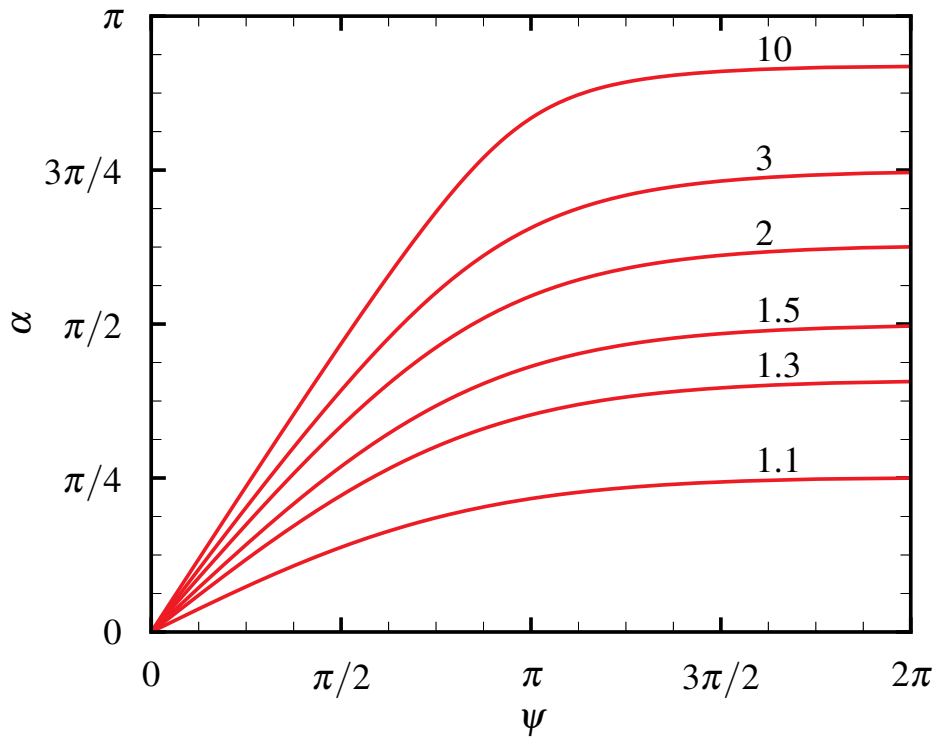

Figure 2.2: Relation between the emission angle α and the bending angle ψ computed using the exact relation shown in Eq. (2.11) for six different emission radii $R/R_{\rm S} = 1.1$, 1.3, 1.5, 2, 3, and 10, which are marked above of the corresponding curves.

Numerical calculations to solve α as a function of ψ, for a given radius, can be made after making few variable transformations to the integral (2.9) (see the appendix in Salmi et al. 2018). The resulting relation between α and ψ for different radii is presented in Fig. 2.2. We note that the relation depends only on the compactness of the star via $R/R_{\rm S}$, and the most compact cases shown ($R/R_{\rm S} \leq 1.5$) are not allowed for NSs, since otherwise the causality would break inside the star (speed of sound in the dense matter would be higher than the speed of light). Nevertheless, photons emitted to higher than a critical angle (which depends on the compactness) can not escape to the observer. As an alternative, one could also use the approx-

imate analytical expressions for the relation between α and ψ, which are presented, for example, by Beloborodov (2002) or Poutanen (2020a). When α is determined, we know also the emission angle σ from Eq. (2.6), and after converting the angles to the frame co-rotating with the spot, we can compute the intensity of photons emitted to that direction (see Sect. 2.3).

As mentioned, the description of light bending using Schwarzschild geometry neglects the rotational effects of the NS. Therefore, a common approach to account for the fast rotation of the star, has been to apply special relativistic corrections to the angles, energies, photon arrival times, and to the observed area of the spot when transferring the quantities from the observer frame to the co-rotating frame of the spot (Poutanen & Beloborodov 2006). The Doppler factor can be formulated as

$$\delta = \frac{1}{\Gamma(1 - \beta \cos \xi)}, \tag{2.13}$$

where Γ is the Lorentz factor for the velocity β (in units of c) of the star at $R(\theta)$, and ξ is the angle between the velocity and the direction of the emitted photon. Since the velocity depends on the radius of the star, additional information (besides the light bending) of the NS radius is encoded in the observed pulse profiles. For example, the emission angle σ in the observer frame can be related with the emission angle σ' in the co-rotating frame, as

$$\cos \sigma' = \delta \ \cos \sigma. \tag{2.14}$$

Another relativistic effect to take into account is the different travel times of emitted photons to the observer, which depend on the position of the emitting point (Pechenick et al. 1983). The phase φ when the photon arrives to the observer differs from the emission phase ϕ by

$$\varphi = \phi + 2\pi\nu\Delta t, \tag{2.15}$$

where Δt is the time delay relative to a photon that is emitted with a reference impact parameter from a reference radius (the choice of the reference here is arbitrary). For a complete set of equations, including the calculation of Δt, we refer, for example, to Poutanen & Beloborodov (2006), Salmi et al. (2018) and Bogdanov et al. (2019).

For the most rapidly rotating stars, accounting for the rotational metric-

deformation effects (beyond the assumed Schwarzschild approximation) might also be relevant (Bauböck et al. 2012, 2013; Nättilä & Pihajoki 2018; Vincent et al. 2018) although generally computationally expensive for statistical inference applications. However, Suleimanov et al. (2020) recently showed that the simplified Schwarzschild description for the light bending could still be kept if only correcting the gravitational redshift and Doppler boost to approximately account for the frame dragging and quadrupole moment of a NS.

2.3 Observed flux

As discussed in the previous two sections, after knowing the emission angle σ' (measured in the frame co-moving with the spot), we can determine the specific intensity of photons I_E emitted to the angle σ' and observed at energy E. However, the models for angular dependence of the intensity vary between different types of pulsars and are also generally energy-dependent. Therefore, the pulses profiles appear to be different at different photon energies and can not be considered without modelling also the spectral distribution of radiation.

The flux measured by the distant observer from an infitesimal spot (at photon energy E) is obtained from

$$\mathrm{d}F_E = I_E \mathrm{d}\Omega, \tag{2.16}$$

where $\mathrm{d}\Omega$ is the solid angle covered by the spot on the sky. It depends on the light bending and relativistic corrections, and can be expressed as (at a distance D from the star) (Morsink et al. 2007)

$$\mathrm{d}\Omega = \frac{\mathrm{d}S' \cos\sigma'}{D^2} \frac{1}{1-u} \frac{\mathrm{d}\cos\alpha}{\mathrm{d}\cos\psi}, \tag{2.17}$$

where $\mathrm{d}S'$ is the area of the spot in the co-rotating frame. When considering finite-sized spots, one needs to evaluate the fluxes (and e.g. the light bending) separately in a number of small sub-spots, and then integrate over the spot surface. In case of two hot spots on the NS surface (located at the opposite poles if the magnetic field is dipolar), we integrate over both spots. However, for some NSs (like SAX J1808.4−3658) the other spot is expected to be hidden by the accretion disk and may thus be neglected

(Ibragimov & Poutanen 2009).

The intensity I_E, shown in Eq. (2.16), can be calculated by taking into account the gravitational redshift and Doppler boost of the photon energies (Misner et al. 1973; Rybicki & Lightman 1979):

$$I_E = (\delta\sqrt{1-u})^3 I'_{E'}(\sigma'), \tag{2.18}$$

where $I'_{E'}(\sigma')$ is the intensity at the co-moving frame of the spot. This quantity depends on the physical conditions above the NS surface. In case of AMPs, an accretion shock is expected to form above the hot spot and to affect the angular and spectral distribution of the photon intensity. Due to the lack of self-consistent physical models for the accretion shock, only empirical models for the spectrum and parametrised formulation for the beaming pattern has recently been applied (Steiner et al. 2009; Salmi et al. 2018). In case of RMPs, the emission pattern from the hot spot can be estimated using existing NS atmosphere models (Zavlin et al. 1996; Heinke et al. 2006; Suleimanov & Werner 2007; Ho & Heinke 2009; Haakonsen et al. 2012). In Chapter 3 we discuss how these models can be employed and improved in order to attain robust mass and radius constraints for NSs using pulse profile modelling.

2.4 Mass and radius constraints

The pulse shape model presented in the previous sections can be combined with Bayesian inference in order to constrain parameters of the model, such as the NS mass and radius (see e.g. Lo et al. 2013; Miller & Lamb 2015). Bayesian analysis is a commonly used mathematical tool to evaluate the credible limits and the most probable values for the model parameters when fitting the data. It can be used together with Markov Chain Monte Carlo (MCMC) methods to integrate uncertainties over the parameter space (Sharma 2017). In particular, we are interested in the credible regions for the mass and radius, which are computed by marginalising the uncertainties in other parameters.

In case of pulse profile modelling, Bayesian methods were first applied in order to study synthetic data that could be observed by future X-ray telescopes (Lo et al. 2013; Miller & Lamb 2015). In our work (paper I, i.e. Salmi et al. 2018), we have confirmed the robustness of our method using synthetic data, but also applied to it to the existing data of AMP SAX

J1808.4−3658 detected by RXTE. Bayesian inference has also been applied in papers II (Salmi et al. 2019), IV (Loktev et al. 2020), and V (Salmi et al. 2020a) to study different atmosphere and polarization models and their effects on the mass and radius constraints (see discussion in the following chapters). Recently, mass and radius constraints for RMPs and NS EoS constraints were obtained using the novel observations of the RMP PSR J0030+0451 by the Neutron star Interior Composition ExploreR (NICER) (Miller et al. 2019; Raaijmakers et al. 2019; Riley et al. 2019).

The complete description of Bayesian methods can not be fully presented here. However, for a brief summary, we note that the most important relation between different probability distributions in Bayesian theorem can be presented as (Grinstead & Snell 1997)

$$p(\mathbf{y}|\mathcal{D}) \propto p(\mathcal{D}|\mathbf{y})p(\mathbf{y}), \tag{2.19}$$

where $p(\mathbf{y}|\mathcal{D})$ is the (posterior) probability distribution of the model parameters given the data, $p(\mathcal{D}|\mathbf{y})$ is the likelihood or the probability distribution of the (pulse profile) data given the parameters, and $p(\mathbf{y})$ is the prior probability distribution of the parameters. A prior distribution can be used to describe the previously known information about the system, assumed to be simply uniform, or estimated as non-informative as possible (see e.g. Jeffreys 1946). The likelihood of the data, on the other hand, is obtained from the fitting algorithm, which calculates the probability of the observed number of photons (in each energy-phase bin) to be produced with a given set of model parameters. Usually, a normal distribution can be assumed to describe the probability distribution around the modelled number of photons. Different sampling algorithms, for example MCMC methods or multimodal nested sampling, may be used to find the most probable parameter values (Goodman & Weare 2010; Feroz et al. 2009).

Further details of the posterior probability computation are presented in paper I. In the same paper, we also show that accurate constraints for NS radius can be obtained (even with RXTE) if the mass is a priori known (see Fig. 2.3) and further constraints are achievable if assuming additional information from the upcoming X-ray polarization measurements (see also Chap. 4). However, considering mass as a free parameter results in small masses and radii not realistic for any modern EoS, which we interpret to be an outcome from a non-perfect model for the AMP. Especially, the used parameterisation of the beaming pattern may not capture its exact

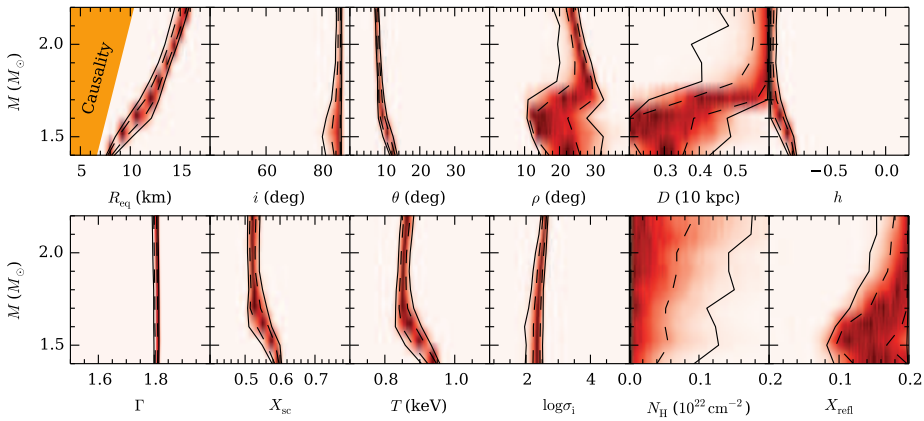

Figure 2.3: Posterior probability distributions for NS parameters for RXTE SAX J1808.4−3658 data, where a fixed mass grid has been used. The solid contour shows a 95% and the dashed contour a 68% highest posterior density credible region. The colours, contours, and symbols are explained in paper I. Taken from Salmi et al. (2018).

energy-dependent nature. In case of RMPs, the surface emission pattern is known more accurately, and plausible mass and radius constraints of $R_{\rm eq} \approx 13^{+1}_{-1}$ km and $M \approx 1.4^{+0.2}_{-0.2}\,{\rm M}_\odot$ were obtained using the recent NICER observations (Riley et al. 2019; Miller et al. 2019). However, these models also resulted in complicated shapes and locations of the emitting hot spots implying a non-dipolar magnetic field configuration. In our work, we have (so far) restricted ourselves mainly to circular and antipodal spots, but studied the surface emission pattern of RMPs in more detail. We have developed more realistic atmosphere models (see paper III, i.e. Salmi et al. 2020b, and the next chapter), which can significantly affect the beaming and therefore also the mass and radius constraints (inspecting the latter is left as a future study).

Chapter 3

Modelling the atmosphere of a neutron star

In this chapter, we will the discuss modelling of the NS atmosphere (see papers II and III), which can be used to obtain the angular and energy dependence of the intensity required in pulse profile modelling ($I'_{E'}(\sigma')$ in Eq. (2.18)). We focus on the atmospheres of RMPs due to the expectations of less complicated physics compared to AMPs (lack of radiation re-processing in an accretion column). We begin by introducing the concept of radiative transfer describing how the radiation is transmitted through a medium. Especially, the effect of Compton scattering during the process is summarised. We finish the chapter by explaining the scheme for our recent iterative atmosphere models; how a self-consistent solution for the atmosphere structure and emergent spectrum can be achieved.

3.1 Radiative transfer

Radiative transfer is a process, in which a beam of radiation travels in a medium. In principle, radiation can lose energy due to absorption, gain energy due to emission, and redistribute energy (to different directions) by scattering. The process can be described using the non-magnetic radiative transfer equation with plane-parallel (one-dimensional) approximation (Mihalas 1978; Zavlin & Pavlov 2002):

$$\mu \frac{\mathrm{d}I(E,\mu)}{\mathrm{d}\tau(E,\mu)} = I(E,\mu) - S(E,\mu), \tag{3.1}$$

where $\mu = \cos\sigma'$, $S(E,\mu)$ is the source function,

$$\mathrm{d}\tau(E,\mu) = -[\sigma_{\mathrm{SC}}(E,\mu) + k(E)]\rho\mathrm{d}z \tag{3.2}$$

is the optical depth element, $\sigma_{\mathrm{SC}}(E,\mu)$ is the scattering opacity, $k(E)$ is the 'true' absorption opacity, ρ is the gas density, and z is the geometrical depth. We note that here, and henceforth, $I'_{E'}(\sigma')$ is replaced with $I(E,\mu)$ for simplicity (the prime is also dropped from other quantities since we consider now physics only in the frame co-moving with the spot). The sum of the scattering and absorption opacities is the total radiative opacity and it depends on both temperature-density structure of the atmosphere and on the radiation field itself (due to induced scattering included in $\sigma_{\mathrm{SC}}(E,\mu)$). The calculation and significance of the scattering opacity are outlined in the next section. In addition, the source function $S(E,\mu)$ can be represented as a sum of thermal part and scattering part. The latter is also affected by the incident radiation $I(E,\mu)$. Therefore, Eq. (3.1) for $I(E,\mu)$ cannot be trivially solved, but iterative methods must be used instead.

Let us now briefly introduce the procedure that we use to solve the radiative transfer equation for a given temperature and density structure of the atmosphere. The first step is to make an initial guess for the source function: for example, only the thermal part of the source function. For a given optical depth and source function, the formal solution of Eq. (3.1) is obtained using the short-characteristic method (Olson & Kunasz 1987), where intensities from the adjacent points are utilised in order to obtain the inward and outward directed intensities ($I_i^-(E,\mu)$ and $I_i^+(E,\mu)$ respectively) at some point i in the optical depth grid:

$$I_i^-(E,\mu) = I_{i-1}^-(E,\mu)\exp\left[-(\tau_i^- - \tau_{i-1}^-)/|\mu|\right] + \int_{\tau_{i-1}^-}^{\tau_i^-} S^-(t,E,\mu)\exp\left[-(\tau_i^- - t)/|\mu|\right]\mathrm{d}t/|\mu| \tag{3.3}$$

and

$$I_i^+(E,\mu) = I_{i+1}^+(E,\mu)\exp\left[-(\tau_{i+1}^+ - \tau_i^+)/\mu\right] + \int_{\tau_i^+}^{\tau_{i+1}^+} S^+(t,E,\mu)\exp\left[-(t - \tau_i^+)/\mu\right]\mathrm{d}t/\mu. \tag{3.4}$$

Here the integrals can be computed as sums using interpolation coefficients

derived by Olson & Kunasz (1987). Providing inner and outer boundary conditions, the solution for the intensity at full optical depth grid is obtained. However, as explained above, the intensity affects the source function, which should be re-calculated as it, in general, deviates now from the initial assumption. New intensities and source functions are iteratively computed until the relative change in them is smaller than a pre-determined accuracy. For an efficient convergence the iterations can be performed by making additional corrections to the intensities at every iteration (see Suleimanov et al. (2011) for the accelerated Λ-iteration method).

As explained in this section, the radiative transfer equation can be used to solve for the emitted intensities (for different emission angles σ and photon energies E), when the structure of the atmosphere is known. However, to solve the structure, another iterative approach is required and it is described in Sect. 3.3.

3.2 Compton scattering

Let us next discuss the photon-electron scattering process in more detail, as it is one of the essential phenomena studied in papers II and III. To determine the electron scattering opacity $\sigma_{\rm SC}(E, \mu)$, shown in Eq. (3.2), one needs to evaluate how many of the photons propagating to a direction μ_1 with an energy E_1 are scattered to the direction μ and energy E. In case of temperatures much lower than the corresponding electron rest mass energy ($kT \ll m_{\rm e}c^2$, i.e. $T \ll 6 \times 10^9$ K), the scattering can be described by the Thomson approximation where scattering is elastic and photon energies do not change. This approximation is also used in many atmosphere models of RMPs (see e.g. Haakonsen et al. 2012) that typically have effective temperatures about 1 MK, in which the exact Compton formalism of photon-electron scattering might, however, still be important (see paper II). Especially, in the atmospheres heated in the surface layers by bombarding particles (see paper III), the outer layers may reach very high temperatures and the exact Compton treatment can influence the observed emission properties.

In order to account for the inelastic photon-electron (Compton) scattering effects, we calculate the redistribution function $R(E, \mu; E_1, \mu_1)$, which expresses the probability of a particular transition. It can be calculated at various degrees of accuracy: the fully relativistic and exact redistribu-

tion function is valid for any photon energies and electron temperatures (Aharonian & Atoyan 1981; Nagirner & Poutanen 1993, 1994; Poutanen & Svensson 1996; Suleimanov et al. 2012), but for RMPs also approximate functions can be applied. The latter may include, for example, an angle-averaged redistribution function, or assume isotropic scattering in the electron rest frame (Arutyunyan & Nikogosyan 1980; Poutanen 1994). Finally, integration over all possible arrival directions μ_1 and energies E_1 is made to attain the scattering opacity for the required μ and E. In addition, the scattering part of the source function $S(E, \mu)$ must also be computed using a similar approach. Since both the scattering opacity and source function depend on the incident radiation field, they are re-calculated for every radiative transfer iteration (explained in Sect. 3.1). Fortunately, the redistribution function depends only on the temperature of the surrounding electrons and thus needs to be calculated only once for a given atmospheric structure.

3.3 Atmosphere models

Let us now discuss how a self-consistent temperature structure and emergent spectrum from a NS atmosphere can be obtained and how our work has enhanced these models. As explained in Sect. 3.1, the radiative transfer equation is iteratively solved for the temperature and density given as a function of atmospheric depth. For an initial guess, we can use the so-called Gray atmosphere model (Eddington 1916; Rybicki & Lightman 1979). However, if the obtained emergent radiation is found not to satisfy the condition of energy balance (see definition later in Eq. (3.6)), corrections to the initial temperature profile are made and calculations repeated. Also, equations governing atmospheric pressure and density are needed in order to estimate the corrected density profile of the atmosphere. For example, the pressure at each depth is determined using hydrostatic balance equation:

$$\frac{1}{\rho}\frac{\mathrm{d}P}{\mathrm{d}r} = -g - g_{\mathrm{ram}} + g_{\mathrm{rad}}, \tag{3.5}$$

where P is the gas pressure, g is the surface gravity, g_{rad} is the radiative acceleration (defined in Suleimanov et al. 2012), and g_{ram} is a ram pressure acceleration required when accounting for the inflow of heating particles

(Suleimanov et al. 2018). In addition, the ideal gas law can be used to calculate the number densities of atmospheric particles based on the already known pressure and temperature.

Here we note, that we consider only fully ionised hydrogen atmospheres for RMPs, which is justified since the short gravitational stratification timescale is expected to leave only the lightest elements in the layers which determine the features of the emerging radiation (Alcock & Illarionov 1980; Zavlin & Pavlov 2002). Therefore, calculations of ionisation and excitation states of different elements are not necessary, contrarily to the accretion-heated atmospheres where heavier elements exist and Boltzmann and Saha equations should be applied in order to obtain number densities of different particles (Hummer & Mihalas 1988; Hubeny et al. 1994). Also, before solving the radiative transfer equation, absorption opacities must still be evaluated ($k(E)$ shown in Eq. (3.2)). For that purpose, we consider the free-free opacity as the only source of absorption opacity (use the Kramers' opacity law), neglecting the bound-free transitions of ions heavier than hydrogen.

As already mentioned, once the radiative transfer is solved, the proposed emitted radiation is compared against the energy balance condition, and corrections to temperatures at each depth are performed. Pressures, number densities, opacities, and radiative transfer equation are re-computed until a converged and self-consistent model is found (see Kurucz 1970, for further details of the method). For a heated atmosphere (see paper III), the energy balance condition reads as

$$2\pi \int_0^\infty \mathrm{d}E \int_{-1}^{+1} [\sigma(E,\mu) + k(E)][I(E,\mu) - S(E,\mu)]\mathrm{d}\mu = -Q^+, \qquad (3.6)$$

where Q^+ is the local energy dissipation rate of the penetrating particles. It depends on the energy distribution of the bombarding particles (consisting of electrons and positrons) and how efficiently the energy is dissipated at different depths of the atmosphere. The particles lose their energy primarily via Coulomb collisions with atmospheric electrons and by emitting bremsstrahlung radiation (see Haug 2004; Solodov & Betti 2008, and paper III). In case of a classical deep-heated atmosphere, all the energy is assumed to be released in very deep layers, and thus $Q^+ = 0$ is used at all the depths that are modelled. Furthermore, the energy balance condition of Eq. (3.6) is not applied at every depth in the same form, but an integral

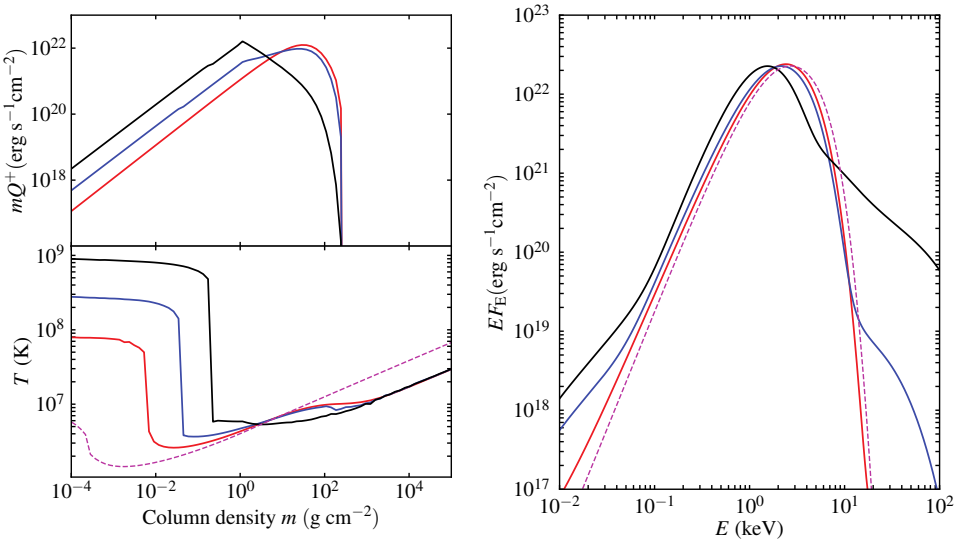

Figure 3.1: Atmosphere structure (*left*) and the spectrum of escaping radiation (*right*). *Left panels*: energy loss of the return current mQ^+ and the temperature T as functions of the column density m. The dashed magenta curves correspond to the standard results without external heating. Red, blue, and black solid curves correspond to the heated models with varying power-law slope of the energy distribution of the bombarding particles, as specified in Fig. 4 of Salmi et al. (2020b), except here we show only those models where all energy loss mechanisms, including bremsstrahlung radiation, are taken into account.

form of it (describing the radiation flux) is applied at low depths in order to maximise the efficiency in the temperature corrections (see Kurucz 1970; Suleimanov et al. 2018, and paper III).

The formalism explained above, takes into account the possibility of the in-falling pair plasma to heat the atmosphere directly in its different layers. This approach has previously been applied for strongly magnetised NSs (González-Caniulef et al. 2019), accreting NSs (Deufel et al. 2001; Suleimanov et al. 2018), and for RMPs with a simplified model atmosphere

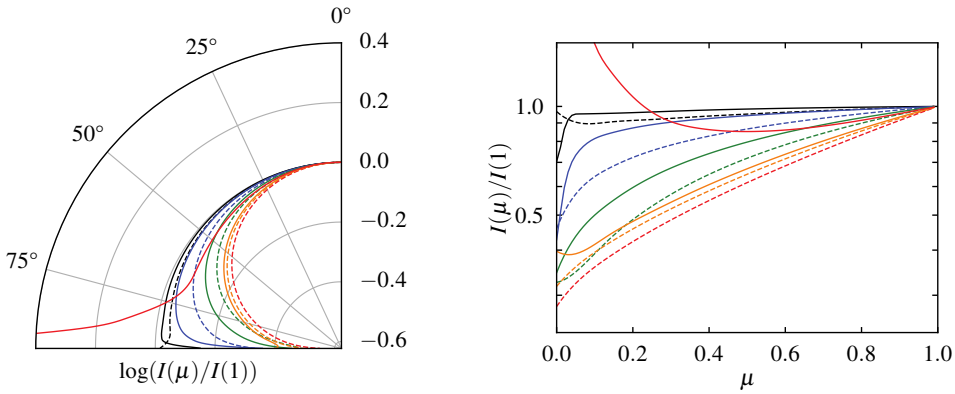

Figure 3.2: Angular dependence of the specific intensity in polar (*left*) and Cartesian (*right*) coordinates for two of the atmosphere models presented in Fig. 3.1. The dashed curves show the emission patterns for non-heated atmosphere model (corresponding to the magenta dashed lines in Fig. 3.1), and the solid curves show the patterns for a heated atmosphere model (corresponding to the blue curves in Fig. 3.1). The results are presented for photon energies 0.1, 0.3, 1, 3, and 10 keV, shown by black, blue, green, orange, and red colours, respectively. This figure corresponds to the middle panel of Fig. 8 in Salmi et al. (2020b), except here we account also for the bremsstrahlung radiation.

(Bauböck et al. 2019). In paper III, we studied return-current-heating effects of RMPs using the full atmosphere model and found that effects on the observed spectra and beaming pattern can be extremely significant for the analysis of pulse profiles observed by NICER. However, previous research has usually assumed a radiative equilibrium which is correct only if the penetrating particles deposit their energy at very deep layers. Comparison between different atmosphere models is shown in Fig. 3.1. We see that those models, where the shallow layers are most heated, produce a significant excess in the radiated spectrum at both low and high photon energies and also the peak of the thermal radiation is shifted. The difference in the beaming pattern between the standard and one of the heated atmosphere models (corresponding the blue lines in Fig. 3.1) is demonstrated in Fig. 3.2. We notice that the angular dependence of radiation deviates highly

from the standard model for the highest photon energies but can also differ tens of per cent even for the thermal part of the spectrum. This discrepancy would produce a significantly different pulse profile.

The energy distribution of the penetrating particles (produced in pairs in pulsar magnetosphere), is still highly uncertain, and the low-energy particles may, indeed, deposit their energy at shallow layers. Models and simulations for slowly rotating pulsar magnetospheres exist (Timokhin & Arons 2013; Chen & Beloborodov 2014; Cerutti & Beloborodov 2017; Philippov & Spitkovsky 2018), but for millisecond pulsars the already large uncertainties are still increased. In the atmosphere model of paper III, the energy distribution of particles is parametrised, allowing a more robust study of the emergent radiation and NS parameter constraints. On the other hand, the model can also be used to indirectly probe the still unknown structure and pair-production physics of the pulsar magnetospheres.

Chapter 4

X-ray polarimetry constraining EoS of dense matter

Until now, we have discussed how the energy-resolved X-ray pulse profiles from millisecond pulsars can be used in order to obtain constraints for the NS mass and radius (and thus to the EoS of the dense matter inside the star). In addition, future X-ray polarization instruments, like Imaging X-ray Polarimeter Explorer (IXPE) and enhanced X-ray Timing and Polarimetry (eXTP) missions (Weisskopf et al. 2016; Zhang et al. 2016), will also soon open a new window to the NS astrophysics. Instead of observing only the number of X-ray photons at different energy and phase bins, the satellites will enable us to measure the number of photons for different polarization states of the radiation (described by the so-called Stokes parameters I, Q, U and V). The polarized radiation is expected to offer additional information especially of the NS geometry, which should provide also further constraints to the mass and radius (Viironen & Poutanen 2004; Salmi et al. 2018, see also papers IV and V). More precisely, it can efficiently break the degeneracy between the observer inclination i and the co-latitude θ of the emitting hot spot. This is illustrated in Fig. 4.1, where we see that exchanging i and θ does not affect the pulse profile and polarization degree (PD), but the polarization angle (PA) changes completely.

It is known that scattering between photons and electrons creates polarized radiation with PD that depends on the scattering angle (Bellazzini et al. 2010). Since Compton scattering is the main emission mechanism in AMPs, they are suitable candidates for X-ray polarization studies. They

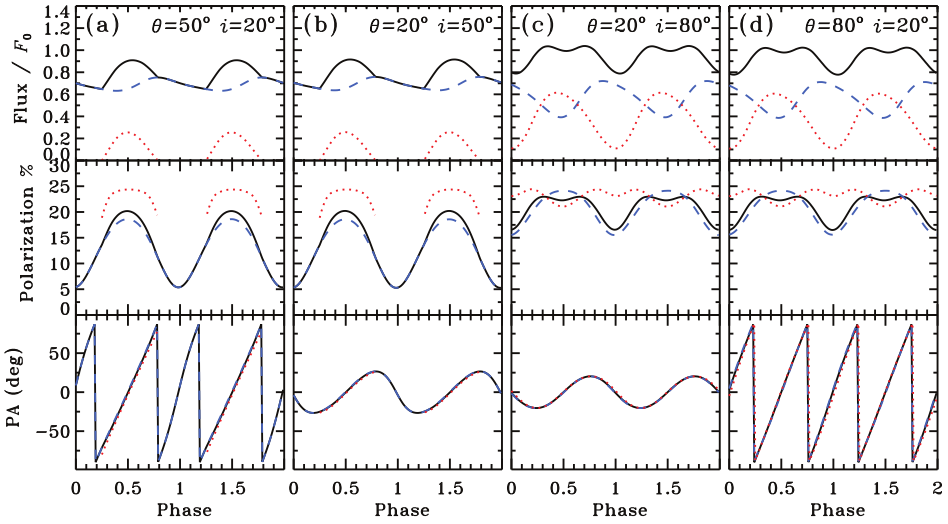

Figure 4.1: Normalised flux, PD, and PA for two small antipodal spots for various observer and magnetic inclinations. Blue dashed curves present the contribution from the primary spot, red dotted curves from the antipodal spot, and black solid lines show the total signal. Taken from Watts et al. (2019), and originally adapted from Viironen & Poutanen (2004), where also other model parameters are defined.

are also luminous enough to be observed in the energy bands of IXPE and eXTP. A model for polarized radiation from AMPs was introduced in Viironen & Poutanen (2004) (see also Sunyaev & Titarchuk 1985). It is based on Comptonization in the Thomson scattering limit for optically thin NS atmospheres. For a more accurate model, one should apply the formalism for Compton scattering in a hot slab (see e.g. Poutanen & Svensson 1996). However, since the exact approach is computationally expensive, we have only considered simplified models when simulating the upcoming polarization observations and NS parameter constraints (see papers IV and V for details).

The models for polarized radiation from electron scatterings in AMP atmospheres provide the Stokes parameters in the co-moving frame of the emitting hot spot. However, it is also important to accurately transform them to the observer frame. For rapidly rotating millisecond pulsars one

must account for the light bending, special relativistic rotation effects, and the oblate shape of the star. The latter effect is for the first time included in the analytical formulas for the PA in paper IV (for a spherical star see Viironen & Poutanen 2004 and Poutanen 2020b). PA describes the change in position of the polarization vector, and it is applied to calculate the Stokes parameters in the observer frame. The obtained Stokes parameters can be compared to the those inferred directly from the observations (Kislat et al. 2015) and used to obtain NS parameter constraints (see paper V). According to our results, the constraints for the NS geometry (based on the simulated IXPE data) can reach such an accuracy, which is enough to improve the NS mass and radius constraints. The launch of the new X-ray polarimeters like IXPE (scheduled launch in 2021) is thus expected to provide a valuable tool for obtaining additional information about the interiors of the NSs.

Chapter 5

Summary of the original publications

5.1 Paper I – Bayesian parameter constraints for NS masses and radii using X-ray timing observations of accretion-powered millisecond pulsars

In this paper, we presented a method to constrain masses and radii of NSs using energy-resolved X-ray pulse profile observations of AMPs. Using two different synthetic data, we showed that additional information on NS geometry (e.g. from the upcoming X-ray polarization measurements) leads to tighter constraints in mass and radius. We also analysed the existing X-ray data of SAX J1808.4−3658 observed by RXTE. When having no prior information of the mass, we found constraints favouring relatively small masses and radii, which are not realistic for most of the modern equation of states. We interpreted this to be an outcome of the model not capable to explain all the features in the data, for example, due to the lack of an accurate and physical atmosphere model of the accreting NS.

5.2 Paper II – Effects of Compton scattering on the neutron star radius constraints in rotation-powered millisecond pulsars

In this paper, we studied how the use of Thomson scattering approximation in atmosphere calculation, instead of full Compton scattering model, affects NS parameter constraints from RMP pulse profile observations of NICER. Our results showed that deviations in some of the inferred results appear if the hot spot has at least a temperature of $T = 3$ MK and if the data is fitted with an inaccurate model. However, the biases were detected only in the size and temperature of the spot, and radius measurements were not affected. This implies that Compton scattering might be unimportant for radius constraints, at least in the case of a similar deep-heated atmosphere model considered here.

5.3 Paper III – Magnetospheric return-current-heated atmospheres of rotation-powered millisecond pulsars

In this paper, we presented a model for return-current-heated atmospheres of RMPs where, instead of deep-heating approximation, the bombarding particles were assumed to dissipate their energy at the various layers of the atmosphere. We employed the full radiative transfer calculation accounting exactly for Compton scattering and considered different energy loss mechanisms of penetrating particles. We found that structure of the atmosphere, the emergent spectrum, and the angular dependence of the radiation may highly deviate from those using the deep-heating approximation. This can have an important effect on the NS parameter constraints obtained recently by NICER. On the other hand, due to parametrisation of the energy distribution of the return current particles, the model can be used to indirectly probe the unknown physics of the millisecond pulsar magnetospheres.

5.4 Paper IV – Oblate Schwarzschild approximation for polarized radiation from rapidly rotating neutron stars

In this paper, we derived new formulas for the PA in case of an oblate millisecond pulsar and demonstrated the importance of the shape of the NS for the analysis of X-ray polarization observations. We obtained first estimates for the constraints of NS geometry, by fitting a synthetic PA profile, and attained information even about the NS radius from pure polarimetry, when considering accurate future measurements of the PA. We also found that assuming an incorrect shape of the star can lead to significant biases in the results, especially in the co-latitude of the hot spot.

5.5 Paper V – Neutron star parameter constraints for accretion-powered millisecond pulsars from the simulated IXPE data

In this paper, we simulated X-ray polarization data that can be obtained with IXPE for a bright AMP like SAX J1808.4−3658. We predicted the measured accuracy in the phase-energy resolved Stokes parameters using different model parameters and lengths of observation. We also fitted the synthetic Stokes profiles using the same model in order to obtain robust estimates for the constraints to the NS geometry. We found that the constraints depend strongly on the true configuration of the observer and the hot spot, but the observer inclination i and the spot co-latitude θ could still be determined with less than 10° accuracy for most of the considered cases. This implies additional constraints also to the NS mass and radius.

5.6 The author's contribution to the publications

Paper I: Bayesian parameter constraints for NS masses and radii using X-ray timing observations of accretion-powered millisecond pulsars

The author contributed to the main idea of the paper, redesigned the pulse profile code to account for the oblate shape of the star, and adjusted the Bayesian fitting code used for calculations. The author also performed the simulations and prepared most of the manuscript.

Paper II: Effects of Compton scattering on the neutron star radius constraints in rotation-powered millisecond pulsars

The author calculated RMP atmosphere models using two different codes (assuming either a Thomson or Compton approach) and employed them to compute and fit pulse profiles. The author also wrote most of the manuscript.

Paper III: Magnetospheric return-current-heated atmospheres of rotation-powered millisecond pulsars

The author contributed to developing the model for return-current-heated atmospheres, constructed the code used for calculations, and performed all the atmosphere computations. The author also prepared most of the manuscript.

Paper IV: Oblate Schwarzschild approximation for polarized radiation from rapidly rotating neutron stars

The author participated in deriving and confirming the new PA equations and conducted the Bayesian analysis that was used to approximate parameter constraints and the effects of the shape of the star. The author also contributed to preparing the manuscript together with V. Loktev. The author's contribution covers approximately 30% of the total amount of work.

Paper V: Neutron star parameter constraints for accretion-powered millisecond pulsars from the simulated IXPE data

The author contributed to the main idea of the paper, expanded and applied the software tools for simulation of polarization data, and performed the calculation of Bayesian parameter constraints. The author prepared most of the manuscript.

Chapter 6

Future studies

There are several apparent projects for future studies originating from the work done in my doctoral studies. One of them is to apply the heated atmosphere model, presented in paper III, to precisely study how important it is for pulse profile modelling of RMPs and for obtaining reliable mass and radius constraints. The atmosphere model can be, for example, used when analysing the already existing NICER data, which is also expected soon to be supplemented. These studies will, hopefully, provide more stringent and robust constraints for the NS mass and radius, and thus to the EoS. They may also help in solving the structure and the unknown physics of the pulsar magnetospheres.

The second project is to take advantage of the upcoming X-ray polarization measurements from IXPE and eXTP. Especially, the launch of IXPE is expected to happen in 2021, and our models for the polarized radiation (presented in papers IV and V) are soon going to be essential when analysing the data from AMPs. Fitting the observed Stokes parameters with the theoretical models will most likely give additional constraints for the NS geometry and thus help to determine the EoS.

The third objective is to further develop the atmosphere models also in the case of AMPs. For example, we would like to construct the model for the accretion shock in AMPs and calculate self-consistently the angular distribution of the emerging radiation. This first-principle model would significantly reduce the number of free parameters and would allow getting better mass-radius constraints. Combination of accurate atmosphere models with polarized pulse profile modelling can, therefore, have a major contribution in understanding the properties of the ultra-dense matter inside NSs.

Bibliography

Abbott, B. P., Abbott, R., Abbott, T. D., et al. 2018, Phys. Rev. Lett., 121, 161101

Abbott, R., Abbott, T. D., Abraham, S., et al. 2020, ApJ, 896, L44

Aharonian, F. A. & Atoyan, A. M. 1981, Ap&SS, 79, 321

Al-Mamun, M., Steiner, A. W., Nättilä, J., et al. 2020, arXiv e-prints, arXiv:2008.12817

Alcock, C. & Illarionov, A. 1980, ApJ, 235, 534

AlGendy, M. & Morsink, S. M. 2014, ApJ, 791, 78

Alme, M. L. & Wilson, J. R. 1973, ApJ, 186, 1015

Alpar, M. A., Cheng, A. F., Ruderman, M. A., & Shaham, J. 1982, Nature, 300, 728

Andronic, A., Braun-Munzinger, P., Redlich, K., & Stachel, J. 2018, Nature, 561, 321

Annala, E., Gorda, T., Kurkela, A., Nättilä, J., & Vuorinen, A. 2020, Nature Physics, 16, 907

Annala, E., Gorda, T., Kurkela, A., & Vuorinen, A. 2018, Phys. Rev. Lett., 120, 172703

Arons, J. 1981, ApJ, 248, 1099

Arutyunyan, G. A. & Nikogosyan, A. G. 1980, Soviet Physics Doklady, 25, 918

Bauböck, M., Psaltis, D., & Özel, F. 2013, ApJ, 766, 87

Bauböck, M., Psaltis, D., & Özel, F. 2019, ApJ, 872, 162

Bauböck, M., Psaltis, D., Özel, F., & Johannsen, T. 2012, ApJ, 753, 175

Baym, G., Hatsuda, T., Kojo, T., et al. 2018, Reports on Progress in Physics, 81, 056902

Bellazzini, R., Costa, E., Matt, G., & Tagliaferri, G. 2010, X-ray Polarimetry: A New Window in Astrophysics, Cambridge Contemporary Astrophysics (Cambridge University Press)

Beloborodov, A. M. 2002, ApJ, 566, L85

Bogdanov, S., Lamb, F. K., Mahmoodifar, S., et al. 2019, ApJ, 887, L26

Cadeau, C., Morsink, S. M., Leahy, D., & Campbell, S. S. 2007, ApJ, 654, 458

Capano, C. D., Tews, I., Brown, S. M., et al. 2020, Nature Astronomy, 4, 625

Cerutti, B. & Beloborodov, A. M. 2017, Space Sci. Rev., 207, 111

Chen, A. Y. & Beloborodov, A. M. 2014, ApJ, 795, L22

Cromartie, H. T., Fonseca, E., Ransom, S. M., et al. 2020, Nature Astronomy, 4, 72

Degenaar, N. & Suleimanov, V. F. 2018, in Astrophysics and Space Science Library, Vol. 457, The Physics and Astrophysics of Neutron Stars, ed. L. Rezzolla, P. Pizzochero, D. I. Jones, N. Rea, & I. Vidaña, 185

Deufel, B., Dullemond, C. P., & Spruit, H. C. 2001, A&A, 377, 955

Eddington, A. S. 1916, MNRAS, 77, 16

Feroz, F., Hobson, M. P., & Bridges, M. 2009, MNRAS, 398, 1601

González-Caniulef, D., Zane, S., Turolla, R., & Wu, K. 2019, MNRAS, 483, 599

Goodman, J. & Weare, J. 2010, Communications in Applied Mathematics and Computational Science, Vol. 5, No. 1, p. 65-80, 2010, 5, 65

Greif, S. K., Raaijmakers, G., Hebeler, K., Schwenk, A., & Watts, A. L. 2019, MNRAS, 485, 5363

Grindlay, J. E., Camilo, F., Heinke, C. O., et al. 2002, ApJ, 581, 470

Grinstead, C. M. & Snell, J. L. 1997, Introduction to Probability, 2nd ed (Providence, RI: American Mathematical Society)

Gyulassy, M. & McLerran, L. 2005, Nucl. Phys. A, 750, 30

Haakonsen, C. B., Turner, M. L., Tacik, N. A., & Rutledge, R. E. 2012, ApJ, 749, 52

Haensel, P., Potekhin, A. Y., & Yakovlev, D. G. 2007, Astrophysics and Space Science Library, Vol. 326, Neutron Stars 1: Equation of State and Structure (New York: Springer)

Harding, A. K. & Muslimov, A. G. 2001, ApJ, 556, 987

Haug, E. 2004, A&A, 423, 793

Hebeler, K., Lattimer, J. M., Pethick, C. J., & Schwenk, A. 2010, Phys. Rev. Lett., 105, 161102

Hebeler, K., Lattimer, J. M., Pethick, C. J., & Schwenk, A. 2013, ApJ, 773, 11

Heinke, C. O., Rybicki, G. B., Narayan, R., & Grindlay, J. E. 2006, ApJ, 644, 1090

Ho, W. C. G. & Heinke, C. O. 2009, Nature, 462, 71

Hubeny, I., Hummer, D. G., & Lanz, T. 1994, A&A, 282, 151

Hummer, D. G. & Mihalas, D. 1988, ApJ, 331, 794

Ibragimov, A. & Poutanen, J. 2009, MNRAS, 400, 492

Jeffreys, H. 1946, Proceedings of the Royal Society of London Series A, 186, 453

Kislat, F., Clark, B., Beilicke, M., & Krawczynski, H. 2015, Astroparticle Physics, 68, 45

Kurkela, A., Fraga, E. S., Schaffner-Bielich, J., & Vuorinen, A. 2014, ApJ, 789, 127

Kurucz, R. L. 1970, SAO Special Report, 309

Lattimer, J. M. & Prakash, M. 2001, ApJ, 550, 426

Lattimer, J. M. & Prakash, M. 2004, Sci, 304, 536

Leahy, D. A., Morsink, S. M., & Cadeau, C. 2008, ApJ, 672, 1119

Lo, K. H., Miller, M. C., Bhattacharyya, S., & Lamb, F. K. 2013, ApJ, 776, 19

Loktev, V., Salmi, T., Nättilä, J., & Poutanen, J. 2020, A&A, 643, A84

Martinez, J. G., Stovall, K., Freire, P. C. C., et al. 2015, ApJ, 812, 143

Mihalas, D. 1978, Stellar atmospheres (San Francisco: W.H. Freeman)

Miller, M. C., Chirenti, C., & Lamb, F. K. 2020, ApJ, 888, 12

Miller, M. C. & Lamb, F. K. 1998, ApJ, 499, L37

Miller, M. C. & Lamb, F. K. 2015, ApJ, 808, 31

Miller, M. C., Lamb, F. K., Dittmann, A. J., et al. 2019, ApJ, 887, L24

Misner, C. W., Thorne, K. S., & Wheeler, J. A. 1973, Gravitation (San Francisco: W.H. Freeman and Co.)

Morsink, S. M., Leahy, D. A., Cadeau, C., & Braga, J. 2007, ApJ, 663, 1244

Nagirner, D. I. & Poutanen, J. 1993, A&A, 275, 325

Nagirner, D. I. & Poutanen, J. 1994, Astrophysics and Space Physics Reviews, 9, 1

Nath, N. R., Strohmayer, T. E., & Swank, J. H. 2002, ApJ, 564, 353

Nättilä, J., Miller, M. C., Steiner, A. W., et al. 2017, A&A, 608, A31

Nättilä, J. & Pihajoki, P. 2018, A&A, 615, A50

Olson, G. L. & Kunasz, P. B. 1987, JQSRT, 38, 325

Oppenheimer, J. R. & Volkoff, G. M. 1939, Phys. Rev., 55, 374

Özel, F. 2013, Reports on Progress in Physics, 76, 016901

Özel, F. & Freire, P. 2016, ARA&A, 54, 401

Pechenick, K. R., Ftaclas, C., & Cohen, J. M. 1983, ApJ, 274, 846

Philippov, A. A. & Spitkovsky, A. 2018, ApJ, 855, 94

Pihajoki, P., Mannerkoski, M., Nättilä, J., & Johansson, P. H. 2018, ApJ, 863, 8

Poutanen, J. 1994, JQSRT, 51, 813

Poutanen, J. 2008, in AIP Conf. Ser., Vol. 1068, A Decade of Accreting Millisecond X-ray Pulsars, ed. R. Wijnands, D. Altamirano, P. Soleri, N. Degenaar, N. Rea, P. Casella, A. Patruno, & M. Linares, 77–86

Poutanen, J. 2020a, A&A, 640, A24

Poutanen, J. 2020b, A&A, 641, A166

Poutanen, J. & Beloborodov, A. M. 2006, MNRAS, 373, 836

Poutanen, J. & Gierliński, M. 2003, MNRAS, 343, 1301

Poutanen, J. & Svensson, R. 1996, ApJ, 470, 249

Raaijmakers, G., Greif, S. K., Riley, T. E., et al. 2020, ApJ, 893, L21

Raaijmakers, G., Riley, T. E., Watts, A. L., et al. 2019, ApJ, 887, L22

Radhakrishnan, V. & Srinivasan, G. 1982, Current Science, 51, 1096

Riley, T. E., Watts, A. L., Bogdanov, S., et al. 2019, ApJ, 887, L21

Ruderman, M. A. & Sutherland, P. G. 1975, ApJ, 196, 51

Rybicki, G. B. & Lightman, A. P. 1979, Radiative processes in astrophysics (New York: Wiley-Interscience)

Salmi, T., Loktev, V., Korsman, K., et al. 2020a, A&A, in press, arXiv:2009.09744

Salmi, T., Nättilä, J., & Poutanen, J. 2018, A&A, 618, A161

Salmi, T., Suleimanov, V. F., Nättilä, J., & Poutanen, J. 2020b, A&A, 641, A15

Salmi, T., Suleimanov, V. F., & Poutanen, J. 2019, A&A, 627, A39

Sharma, S. 2017, ARA&A, 55, 213

Silva, H. O., Pappas, G., Yunes, N., & Yagi, K. 2020, arXiv e-prints, arXiv:2008.05565

Solodov, A. A. & Betti, R. 2008, Physics of Plasmas, 15, 042707

Steiner, J. F., Narayan, R., McClintock, J. E., & Ebisawa, K. 2009, PASP, 121, 1279

Stergioulas, N. 2003, Living Reviews in Relativity, 6, 3

Stergioulas, N. & Friedman, J. L. 1995, ApJ, 444, 306

Suleimanov, V., Poutanen, J., & Werner, K. 2011, A&A, 527, A139

Suleimanov, V., Poutanen, J., & Werner, K. 2012, A&A, 545, A120

Suleimanov, V. & Werner, K. 2007, A&A, 466, 661

Suleimanov, V. F., Poutanen, J., & Werner, K. 2018, A&A, 619, A114

Suleimanov, V. F., Poutanen, J., & Werner, K. 2020, A&A, 639, A33

Sunyaev, R. A. & Titarchuk, L. G. 1985, A&A, 143, 374

Timokhin, A. N. & Arons, J. 2013, MNRAS, 429, 20

Tolman, R. C. 1934, Proceedings of the National Academy of Science, 20, 169

Viironen, K. & Poutanen, J. 2004, A&A, 426, 985

Vincent, F. H., Bejger, M., Różańska, A., et al. 2018, ApJ, 855, 116

Watts, A. L., Andersson, N., Chakrabarty, D., et al. 2016, Reviews of Modern Physics, 88, 021001

Watts, A. L., Yu, W., Poutanen, J., et al. 2019, Science China Physics, Mechanics, and Astronomy, 62, 29503

Weisskopf, M. C., Ramsey, B., O'Dell, S., et al. 2016, in Proc. SPIE, Vol. 9905, Space Telescopes and Instrumentation 2016: Ultraviolet to Gamma Ray, 990517

Wijnands, R. & van der Klis, M. 1998, Nature, 394, 344

Zampieri, L., Turolla, R., Zane, S., & Treves, A. 1995, ApJ, 439, 849

Zavlin, V. E. 2006, ApJ, 638, 951

Zavlin, V. E. 2007, Ap&SS, 308, 297

Zavlin, V. E. & Pavlov, G. G. 2002, in Neutron Stars, Pulsars, and Supernova Remnants, ed. W. Becker, H. Lesch, & J. Trümper, 263

Zavlin, V. E., Pavlov, G. G., & Shibanov, Y. A. 1996, A&A, 315, 141

Zel'dovich, Y. B. & Shakura, N. I. 1969, Soviet Ast., 13, 175

Zhang, S. N., Feroci, M., Santangelo, A., et al. 2016, in Proc. SPIE, Vol. 9905, Space Telescopes and Instrumentation 2016: Ultraviolet to Gamma Ray, 99051Q

UNIVERSITY OF TURKU

Painosalama Oy, Turku, Finland 2020

ISBN 978-951-29-8277-6 (PRINT)
ISBN 978-951-29-8278-3 (PDF)
ISSN 0082-7002 (Print)
ISSN 2343-3175 (Online)